THE JOURNAL OF PHYSICAL CHEMISTRY C

Article

pubs.acs.org/JPCC

Observing Single, Heterogeneous, One-Electron Transfer Reactions

Stephanie Zaleski,[†] M. Fernanda Cardinal,[†] Jordan M. Klingsporn,[†] and Richard P. Van Duyne*[,†,‡,§]

[†]Department of Chemistry, Northwestern University, 2145 Sheridan Road, Evanston, Illinois 60208, United States

[‡]Department of Biomedical Engineering, Northwestern University, 2145 Sheridan Road, Evanston, Illinois 60208, United States

[§]Program in Applied Physics, Northwestern University, 2145 Sheridan Road, Evanston, Illinois 60208, United States

Supporting Information

ABSTRACT: Understanding electrochemical events on the single-molecule level is crucial for fields such as catalysis and biological systems. A variety of techniques exist to study the electrochemistry of single molecules, but few provide correlated chemical information. Herein, we study the electrochemistry of rhodamine 6G in nonaqueous conditions and demonstrate the first statistic electrochemical single-molecule SERS (EC-SMSERS) proof of single-electron transfer events. We find that the distribution of reduction events is broader than that in a bulk electrochemical experiment. The distribution of the reduction potentials can be explained by molecular reorientation and variations of the local surface site or chemical potential of the Ag nanoparticle. Our results contribute toward understanding electrochemical behavior of single molecules on the nanoscale monitored by SERS and the ultimate goal of controlling single-electron transfer processes.

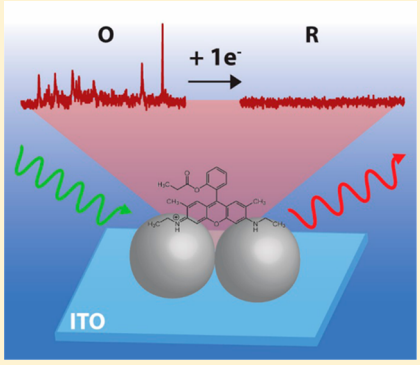

1. INTRODUCTION

The most fundamental event in electrochemistry is the chemically reversible, one-electron, heterogeneous electron transfer (HET) reaction. A HET reaction

$$\mathrm{O} + 1\mathrm{e}^- \underset{k_r}{\overset{k_f}{\rightleftarrows}} \mathrm{R} \qquad (1)$$

involves the oxidized form of the analyte, O, being reduced to its reduced form, R. This reaction is characterized by its standard potential, E^0, and rate constant, k^0. To date, HET reactions have only been studied at the ensemble average level. Consequently, the measured E^0 and k^0 represent an average over many microscopic configurations of O and R and their interactions with the electrode surface.[1−4]

Electrochemical reactions play a central role in numerous fields such as electrocatalysis,[5] energy storage,[6,7] materials synthesis,[8,9] and biological processes,[10−12] averaging different local conditions, i.e., molecule−molecule and molecule−substrate interactions, temperature, and transport properties among others. Single-molecule electrochemistry has been sought after for a long time in order to probe nanoscale local environments. The first demonstration of electrochemistry of a single molecule was reported by Fan and Bard in 1995 by trapping molecules between an insulated Pt/Ir scanning probe tip and an indium tin oxide (ITO) substrate; the bursts in current were attributed to redox of a single molecule moving in and out of the electrode-substrate gap.[13] There was a spike of interest in developing alternative methods to simultaneously detect single molecules and understand their electrochemistry.[14−17] To this end, optical techniques have been combined with electrochemical measurements in order to observe the change in a single molecule as a function of applied potential.[18] Some studies have combined fluorescence spectroscopy with electrochemistry by correlating the fluorescence intensity of a single molecule with applied potential.[19,20] Others used electrochemical scanning tunneling microscopy (EC-STM) to monitor the conformational changes of molecules on a surface as a function of applied potential.[21] Despite the great amount of information gathered from these studies, the techniques used cannot provide detailed chemical information about the changes in electroactive species as a function of applied potential.

Single-molecule SERS (SMSERS) is an ideal technique to investigate the electrochemistry of single molecules because it provides detailed chemical information about the molecular species in question. SMSERS was first claimed as strong intensity fluctuations in an ultralow concentration of Raman-active reporters and with laser excitation on resonance with the electronic absorption of the analyte.[22] Since then, the intensity fluctuation argument for SMSERS has been disproven and groups have explored different single-molecule proofs. The two most commonly used and widely accepted proofs for SMSERS detection are (i) the bianalyte method[23,24] and (ii) the frequency domain, or isotopologue, approach.[25] Both experimental approaches study the statistics of the relative intensities of two distinct molecules (bianalyte approach) or one molecule and its deuterated isotopologue (frequency domain approach) to infer the single-molecule nature of the SERS response. Further investigations focused on achieving (i) SMSERS on various substrates, including colloids,[1,24,26−32] lithographic

Received: October 30, 2015
Revised: November 20, 2015
Published: November 23, 2015

DOI: 10.1021/acs.jpcc.5b10652
J. Phys. Chem. C 2015, 119, 28226−28234

substrates,[33−35] and STM tips using TERS,[36,37] (ii) nonresonant SMSERS,[27] (iii) improved statistics, i.e., a large number of clearly demonstrated SMSERS events.[38] The fundamental aspects of SMSERS have been well-explored,[28,30,39−42] and the next step in SMSERS research is to probe the chemical behavior of single molecules, such as monitoring the pressure-sensitive behavior of single R6G molecules.[43]

The first use of SMSERS to explore electrochemical events was reported by Cortés et al. in 2010. Using the bianalyte approach with dye molecules R6G and Nile blue (NB), the authors demonstrated the feasibility of monitoring single-molecule electrochemistry of NB by SERS.[1] In later work, the authors extended the study to high resolution SMSERS spectra of NB by observing changes in the vibrational frequencies as a function of applied potential. The vibrational changes were attributed to reorientation of the NB molecule in the electrochemical double layer and molecular orientation relative to the nanoparticle surface.[44] Another SMSERS study combined with electrochemistry was reported by Wang et al. using ultralow concentrations of the hemin, an iron porphyrin molecule. In this work, the authors proposed that local thermal fluctuations govern the single electron transfer dynamics of hemin immobilized on Ag nanoparticles.[45] More recently, Willets et al. have demonstrated SMSERS and electrochemistry of NB with a super-resolution microscopy approach, postulating that the NB molecules are sequentially reduced/oxidized on the nanoparticle surface.[4]

From our perspective, the aforementioned reports do not use the most rigorous proof of SM sensitivity; that is, the frequency domain or isotopologue approach,[25] which is therefore our choice for this study. Herein, our primary goal is to understand the electrochemical behavior of R6G on the nanoscale as compared to a bulk electrochemical experiment. First, we characterize the one-electron transfer electrochemistry of R6G both in solution and adsorbed on Ag surfaces at high concentration and coverage in a nonaqueous environment. Second, we demonstrate the first proof of *nonaqueous*, *single-molecule* electrochemistry optically monitored with the *isotopologue* approach of SMSERS. Last, we compare our distribution of EC-SMSERS-detected reduction events to the bulk and elaborate upon the origins of this behavior. We propose that the broadened distribution on the single molecule, single particle aggregate scale is primarily due to variations in the surface site or chemical potential of the Ag nanoparticle where the R6G is bound. We believe that this work, together with previously discussed works, demonstrates the power of SERS as a tool to optically monitor various classes of electrochemical reactions at the single molecule level.

2. EXPERIMENTAL DETAILS

Chemicals. Trisodium citrate dihydrate 90%, silver nitrate +99.99% ($AgNO_3$), sodium chloride +90% (NaCl), tetrabutylammonium perchlorate +99% (TBAP), hydrogen peroxide solution 30% (H_2O_2), ammonium hydroxide solution 28−30% (NH_4OH), (3-mercaptopropyl)trimethoxysilane (MPS) were purchased from Sigma-Aldrich and used without further purification. HPLC grade acetonitrile (≥99.5%) was purchased from Avantor Performance Materials and further purified prior to use by passing through a Pure Process Technology solvent drying system. Milli-Q water with a resistivity higher than 18.2 MΩ cm was used in all preparations.

Deuterated R6G. The synthesis of R6G-d_4 is based on previous conditions given by Zhang et al.[46] and has been reported elsewhere.[25] Standard solutions of R6G-d_0 and R6G-d_4 were prepared and characterized with UV−vis absorbance spectroscopy (Figure S1).

Bulk Electrochemistry. Bulk electrochemical measurements were performed in a capped scintillation vial. An Ag wire (0.25 mm diameter, Alfa Aesar) was utilized as the working electrode and was submerged in solution approximately 1 cm above the Pt wire counter electrode. The reference potential was determined by a nonaqueous Ag wire quasi-reference electrode (QRE) in a tetrabutylammonium perchlorate (TBAP) solution in acetonitrile. A 1 mM R6G solution was prepared in 100 mM TBAP in acetonitrile. For the surface cyclic voltammetry measurements, a polished 2 mm diameter Ag disk electrode (CH Instruments) was incubated in 150 μM R6G-d_0 for 15 min and then gently rinsed with acetonitrile to remove any unbound molecules. The supporting electrolyte solution was degassed with N_2 for 30 min prior to obtaining electrochemical measurements. Electrochemical measurements were performed using a CH Instruments potentiostat (CHI660D).

R6G Neutral Radical Absorbance Characterization. Thin layer cells were prepared by first attaching Ag wire to an ITO coverslip using Ag colloidal paste (Ted Pella). Next, a clean glass coverslip was placed on top and the outsides were sealed with TorrSeal epoxy. The cell was clamped together using reverse-close tweezers and allowed to cure overnight. The cell was placed in a custom-made freeze−pump−thaw (FPT) spectroelectrochemical glass cell with 1 cm optic path length. A 1 mM R6G solution was prepared in 100 mM TBAP in acetonitrile. Four FPT cycles were performed on the solution prior to the measurements. Electrochemical potential was controlled with a CH Instruments potentiostat (CHI660D), and UV−vis extinction spectra were acquired using an Agilent Cary 5000 spectrophotometer. Solution phase CVs were simulated using the cyclic voltammetry fitting mode of DigiElch (version 6.0) simulation software.

Ag Nanoparticle Synthesis. Silver colloids were synthesized using the Lee and Miesel method.[47] Briefly, 90 mg of silver nitrate was dissolved in 500 mL of water, stirred and brought to boil. Once the solution was vigorously boiling, 10 mL of a 1% w/v trisodium citrate solution was added under strong stirring. This solution was boiled for 30 min, removed from the heat, and allowed to cool to room temperature; then the final volume was topped off at 420 mL with ultrapure water. Transmission electron microscopy characterization of the colloid showed spheroidal silver particles of approximately 56 ± 13 nm in diameter. The silver colloid was stored in darkness and used within 1 week.

Sample Cell for EC-SERS. A glass cell for spectroscopic and electrochemical measurements and for FPT of the solvent was custom blown (Reliance Glassware, Elk Grove, IL). The sample cell consists of two inlets for Ag and Pt wire, as well as a no. 5 valve connection (Figure 2A and Figure S2B). The FPT cell consists of a tube for the solvent, and two no. 5 valve connections for connection to the pump and sample cell (Figure S2A).

EC-SERS and EC-SMSERS Sample Preparation. Briefly, an amount of 2 mL of the as prepared Ag colloids was washed and concentrated by two centrifugation steps (2000 rpm, 6 min; supernatant to 5000 rpm 6 min), the pellets were redispersed with 0.5 mL of ultrapure water. For the SERS

DOI: 10.1021/acs.jpcc.5b10652
J. Phys. Chem. C 2015, 119, 28226−28234

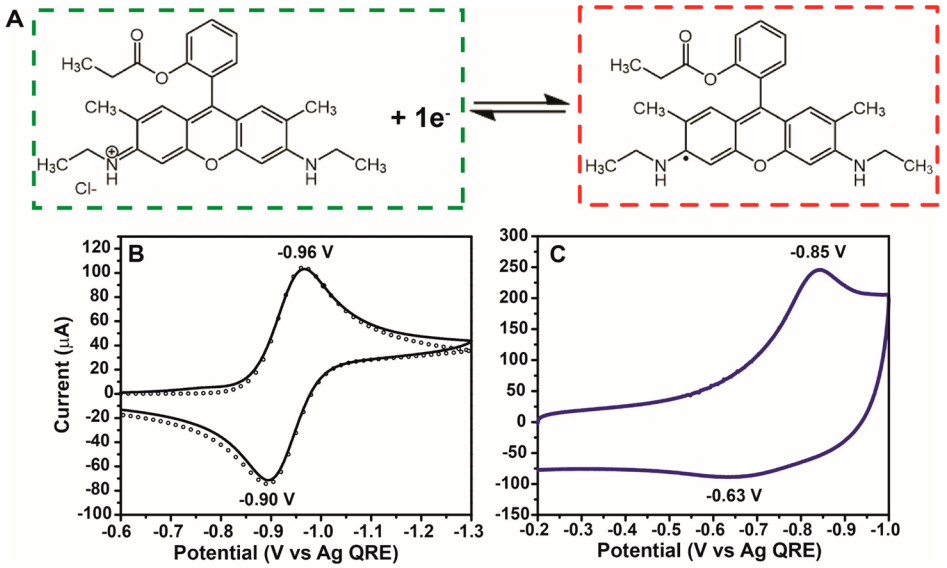

Figure 1. (A) Schematic of heterogeneous one-electron transfer reaction for the reduction of rhodamine 6G cation (green box) to its neutral radical product (red box). (B) 1 mM R6G solution phase CV on Ag working electrode (black trace) and fitted electrochemical simulation data (black circles). (C) Surface CV of high coverage R6G AgNPs on ITO.

sample, to the colloid 100 μL of 1×10^{-5} M total (50 μL of 0.5×10^{-6} M each) of R6G-d_0 and R6G d_4 isotopologues was added and incubated with mild stirring for 1 h. For the SMSERS sample, to the colloid 100 μL of 1×10^{-7} M total (50 μL of 0.5×10^{-8} M each) of R6G-d_0 and R6G-d_4 isotopologues was added and incubated with mild stirring for 1 h. We calculated the maximum R6G/nanoparticle ratio at the SM concentration regime as 3:1, assuming total reduction of silver salt to 30 nm spherical nanoparticles[47] and complete (100%) adsorption of R6G molecules to the particles surface. We assume that R6G/nanoparticle ratio is close to 1:1 in our final experimental conditions, since (i) during the incubation, not all the R6G might adsorb,[22] (ii) after incubation the samples were thoroughly rinsed, and (iii) further desorption of R6G might take place to the electrolyte solution. Later, 0.5 mL of 40 mM NaCl was added to induce nanoparticle aggregation and left overnight before using the sample. ITO coverslips (22 × 22 mm^2, 8−12 Ω, copper busbar, SPI Supplies) were functionalized with (3-mercaptopropyl)trimethoxysilane to covalently attach the Ag nanoparticles. First, the ITO was sonicated in isopropanol for 5 min, then cleaned in a solution of 5:1:1 H_2O/NH_3OH/H_2O_2 for 12 min at 50 °C. Then, 0.5 mL of (3-mercaptopropyl)trimethoxysilane in 50 mL of isopropanol was allowed to react at RT for 5 min. The Ag colloids were then drop casted onto the ITO surface and allowed to dry in an N_2 environment, and then substrates were thoroughly washed to remove any unbound particle or salts. After the ITO is fully dried with N_2, copper tape is placed on the ITO to allow for electrical contact. The sample is then mounted on the SMSERS glass sample cell using TorrSeal epoxy (Duniway Stockroom Corporation, Fremont, CA) and allowed to cure overnight. Next, the cell is placed under vacuum and the supporting electrolyte is transferred in vacuum in order to remove oxygen and water, which quenches radical species and/or cause R6G degradation. The assembled cell was connected to the custom FPT cell which is then connected to a custom built high vacuum line (base pressure of $\sim 10^{-6}$ Torr). The FPT cell is then filled with 10−15 mL performed prior to solvent transfer to the SMSERS cell. After solvent transfer, the SMSERS cell valve was closed and was disconnected from the FPT cell for spectroscopic measurements.

EM Characterization. SEM images were obtained using a FEI Helios NanoLab 600 microscope operating at an acceleration voltage of 3.0 kV and an operating current of 1.4 nA.

Raman Instrumentation. Samples were analyzed on an inverted microscope (Nikon Eclipse Ti-U) with a 100× oil immersion objective and 0.5 numerical aperture. Particle aggregates are initially viewed under dark field illumination with a 0.8−0.95 numerical aperture condenser. To illuminate the entire field of view for SMSERS measurements, a 532 nm CW laser (Millenia VIIIs, Spectra Physics) was focused onto the sample using grazing incidence at an angle of 60° relative to the surface normal. Scattered light was collected from SERS active particles, laser light was filtered (RazorEdge long pass 532 nm filter, Semrock) and focused onto a $^1/_3$ m imaging spectrograph (SP2300, Princeton Instruments). The scattered light was then dispersed (1200 groove/mm grating, 500 nm blaze) and focused onto a liquid nitrogen-cooled CCD detector (Spec10:400BR, Princeton Instruments).

3. RESULTS AND DISCUSSION

I. Electrochemical Characterization of R6G System. Prior to SMSERS measurements, we characterized the bulk electrochemistry of R6G in solution and adsorbed on silver surfaces. R6G undergoes a one-electron transfer, as shown in the schematic in Figure 1A. The solution phase cyclic voltammogram (CV) using a silver wire working electrode is displayed in Figure 1B. In this figure, a peak separation of 64 mV is observed, which is common in diffusion-controlled processes, as well as a good correlation between the experimental (solid line) and simulated (open circles) CVs. Also, we observed a linear relationship between the solution phase CV cathodic peak current and the square root of the scan rate which indicates that this is a reversible, diffusion-controlled process (Figure S3). Next, we studied the electrochemical behavior of R6G adsorbed on Ag nanoparticles (NPs) on ITO, i.e., a high-coverage analog of the electrode used for SMSERS

DOI: 10.1021/acs.jpcc.5b10652
J. Phys. Chem. C 2015, 119, 28226−28234

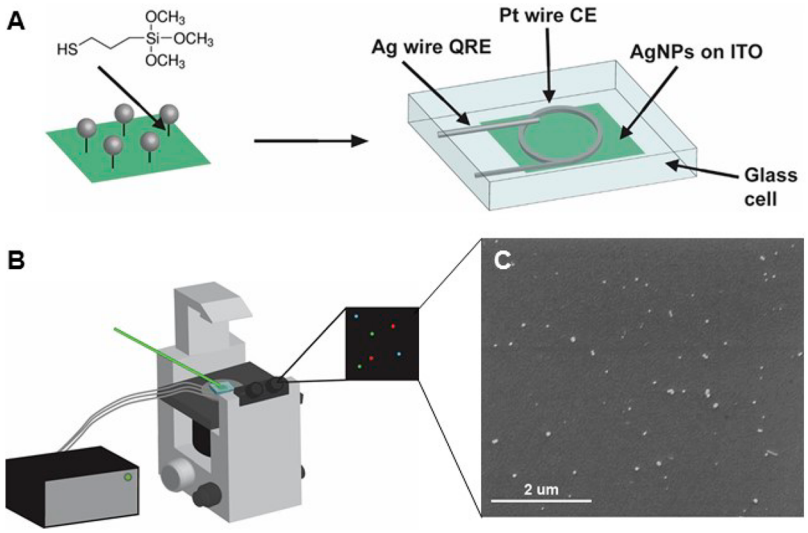

Figure 2. (A) Schematic of AgNP functionalization on an ITO coverslip using MPS and an assembled electrochemistry and spectroscopy glass cell with the functionalized ITO as a working electrode, an Ag wire as the quasi-reference electrode, and a Pt wire as the counter electrode. (B) The assembled spectroscopy glass cell is attached to a potentiostat and then placed on a microscope stage. The laser excitation is focused onto the sample by grazing incidence at an angle of 60° relative to the surface normal. Single nanoparticle aggregates are selected by visually locating and centering a brightly scattering particle in the field of view. (C) Representative SEM image of an AgNP-functionalized ITO substrate at 20 000× magnification.

measurements as shown in Figure 1C. We note that the magnitudes of the reduction and oxidation peaks are not equal, suggesting electrochemical desorption of the R6G neutral radical species after reduction. Additionally, the difference in shape between the solution CV in Figure 1B and surface CV in Figure 1C is due to background capacitance, characteristic of a surface CV.[48] In the case of Ag NPs on ITO as working electrode, when the CV scan rate is increased, we observe a linear relationship with the position of the peak cathodic current, indicative of uncompensated solution resistance (Figure S4, black trace).[48] Also, we confirm that R6G is the surface-bound electroactive species by plotting the cathodic peak current versus scan rate. This relationship is linear which confirms a surface-bound electroactive species[48] (Figure S4, red trace). These results show that R6G has well-behaved electrochemistry as a surface-bound species on an Ag NP surface. This thorough characterization of R6G electrochemistry at high concentration and coverage gives us a solid platform to compare multimolecule and single-molecule reduction potential data.

Later, we characterized the absorbance of the R6G cation and neutral radical species to know if a resonance contribution to the SERS signal is feasible for both species at our experimental conditions (i.e., 532 nm excitation). In order to characterize the relative absorption maxima absorbance of R6G cation and neutral radical, we performed thin-layer chronoabsorptometry. After holding the potential at −0.8 V for 1 min, the cation is fully reduced to the neutral radical, which exhibits an absorption maximum at 413 nm (Figure 3A). This behavior is reversible; after holding the potential at −0.2 V, the absorption trace of the R6G neutral radical is lost and the R6G cation returns.

Lastly, we characterized the electrochemical SERS (EC-SERS) response of R6G on AgNPs covalently attached on ITO (Figure 2A) at multimolecule coverage using 532 nm excitation. The spectral response was monitored from a single nanoparticle aggregate as the potential was stepped from 0 V to −1.2 V and back to 0 V in 0.2 V steps, where the potential was held equal to the length of a spectral acquisition. We observe reversibility in SERS signal as a function of applied potential (Figure 3B), where the SERS signal is lost at −0.8 V and returns at −0.4 V.

From the macroscopic scale electrochemical characterization and multimolecule EC-SERS measurements we conclude that (i) R6G has well-behaved one-electron transfer both in solution and adsorbed on Ag working electrodes and (ii) the electronic resonance of the neutral radical is off-resonance relative to the 532 nm excitation used for EC-SMSERS measurements. Therefore, in this work, the optical readout of a reduction event is defined as the loss of R6G cation SMSER(R)S signal due to the conversion to its neutral radical species.

II. Proof of SMSERS Behavior. SMSERS detection was first statistically proven with the frequency domain proof in our laboratory by Dieringer et al.[25] The benefit of this approach over the bianalyte proof approach is that the analytes have identical surface binding chemistry and Raman scattering cross sections. To this end, equal amounts of R6G-d_0 and R6G-d_4 isotopologues are used in low coverage of the sample. The SMSERS substrate used for these experiments is salt-aggregated Ag Lee and Miesel colloids incubated with 50 μL of 10^{-7} M of each isotopologue, R6G-d_0 and R6G-d_4. The particles are then drop-casted on ITO functionalized with (3-mercaptopropyl)-trimethoxysilane (MPS), which serves as the working electrode. The Ag nanoparticles covalently bind to MPS, as depicted in the schematic in Figure 2A. This ensures that the Ag NPs are electroactive and will not detach from the ITO during SERS measurements. Figure 2C shows a representative SEM image of the Ag colloids functionalized to an ITO coverslip. The SEM images show that the particles are heterogeneous in size and shape and, more importantly, that the aggregates are well distributed on the ITO, enabling SMSERS measurements.

Figure 4A shows representative SMSERS spectra of R6G-d_0 (red line), R6G-d_4 (blue line), and both (green line). In order to differentiate those possible events, i.e., single isotopologue or mixed isotopologues spectrum, we use the characteristic vibrational modes of each molecule. More precisely, there is a

DOI: 10.1021/acs.jpcc.5b10652
J. Phys. Chem. C 2015, 119, 28226−28234

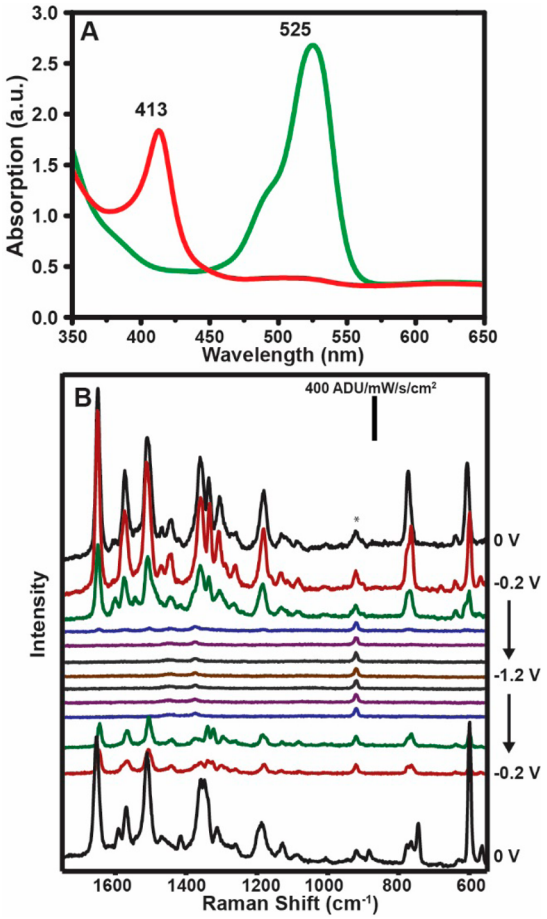

Figure 3. (A) Thin-layer absorbance spectra of 1 mM R6G in 100 mM TBAP in MeCN with no potential applied (green) and after 1 min −0.8 V applied (red). The absorbance measurements were performed with an ITO thin layer working electrode, Ag wire quasi-reference electrode, and a Pt wire counter electrode. (B) EC-SERS of R6G at many molecule coverage where the potential is swept from 0 V (black trace) to −1.2 V (brown trace) in −0.2 V steps, then stepped back to 0 V. The signal is lost at −0.8 V (first purple trace) and returns at −0.4 V (second green trace). The starred peak is due to the acetonitrile solution.

clear spectral distinction between the 601 cm^{-1} peak of R6G-d_0 and the 610 cm^{-1} peak of R6G-d_4; therefore, this spectral region was used to differentiate the isotopologues (Figure 4B). Additionally, R6G-d_4 exhibits a unique doublet feature at 1350 and 1330 cm^{-1} which was also used for molecular identification. SMSERS spectra were acquired from 80 individual particle aggregates for which the events were classified as shown in the histogram in Figure 5B. The ratio of R6G-d_0/both/R6G-d_4 events is 35:5:40 or 7:1:8, confirming single-molecule detection. Our results deviate from a theoretical binomial Poisson distribution for one molecule per particle with a probability ratio of 2.5:1:2.5, and this deviation can be attributed to having less than one R6G molecule per particle, molecules located outside a hot spot during spectral acquisition, molecules not bound to the surface during the incubation time, and/or molecules desorbed in solution.[25]

III. EC-SMSERS Signal Potential Dependence. For electrochemical SMSERS (EC-SMSERS) measurements, the SMSERS signal of each single Ag nanoparticle aggregate was monitored as the potential was stepped from 0 to −1.2 V in 0.1 V intervals and then swept positive from −1.2 to 0 V in 0.1 V intervals. The potential was held constant for the length of SMSERS spectral acquisition (pulse width of 3 s) and the total acquisition time was relatively long (~5 min). A representative trace of the potential step function and the corresponding SMSER signal response are shown in Figure 5A and Figure 5C, respectively. The histogram in Figure 5D corresponds to the R6G SMSERS signal loss events that we understand as the potential at which the R6G cation was reduced to the neutral radical species. Figure 5D only includes single isotopologue signal loss events; we do not include "both" isotopologues spectra. In our experiments, we do not observe SMSERS spectra of the neutral radical species with 532 nm excitation because of the absence of resonance enhancement. The total number of events in Figure 5D (44) is less than that of the histogram in Figure 5B due to signal loss prior to the electrochemical measurements. Sporadic intensity fluctuations, "blinking", and signal loss are common in SMSERS measurements as a result of molecular diffusion, variations of the electric field enhancement, photobleaching, and photochemical effect among others,[23,25] making data acquisition challenging. Figure 5D includes only those particle aggregates in which SMSERS signal was stable for more than ~1 min before the potential step. Overall, it was found that there was significantly less random blinking and signal loss in the liquid cell as compared to previous SMSERS experiments performed in air or nitrogen.

Not included in Figure 5D were 17 other studied particles that did not undergo SMSERS signal loss with the applied potentials. More likely, these particles did not have electrical contact due to defects on the ITO surface or to the particle aggregate requiring a much more negative potential to sufficiently reduce the R6G molecule.

Only two SMSERS signal loss events in Figure 5D had a corresponding signal return, or oxidation. In both cases, the signal return occurred at −0.2 V, which is similar to the behavior observed in the high coverage SERS data (Figure 3B). Possible sources for complete SMSERS signal loss include hot spot reshaping or particle desorption from the ITO, quenching of the R6G radical with water or oxygen traces, or molecular diffusion outside the hot spot. Additionally, this result correlates strongly to the fact that the reduction and oxidation peaks are not of equal magnitude in the surface CV of AgNPs on ITO (Figure 1C) or R6G on polished Ag (Figure 5D). We hypothesize that molecular diffusion or desorption away from the hot spot of the neutral radical species is the main cause of complete SMSERS signal loss after a reduction event. It is also possible that the SMSERS signal is lost due to potential-induced structural changes to the nanoparticle aggregate and therefore loss of SMSERS activity in the hot spot.[49−51]

We attempted to differentiate between possible non-electrochemical desorption of the R6G cation before the potential step (eq 2) from electrochemical desorption of the neutral radical during or after the reduction (eq 3).

$$R6G^{+}_{surf} \underset{k_d}{\overset{k_{ads}}{\rightleftharpoons}} R6G^{+}_{soln} \quad (2)$$

$$R6G^{+}_{surf} + e^{-} \underset{k_d}{\overset{k_{ads}}{\rightleftharpoons}} R6G^{\cdot}_{surf} \underset{k_a}{\overset{k_d}{\rightleftharpoons}} R6G^{\cdot}_{soln} \quad (3)$$

For this, we repeated the measurements stepping the potential only at the non-Faradaic region, from −0.1 to −0.7 V as compared to the surface CV in Figure 1C. We chose to step within this potential window because there should be few

DOI: 10.1021/acs.jpcc.5b10652
J. Phys. Chem. C 2015, 119, 28226−28234

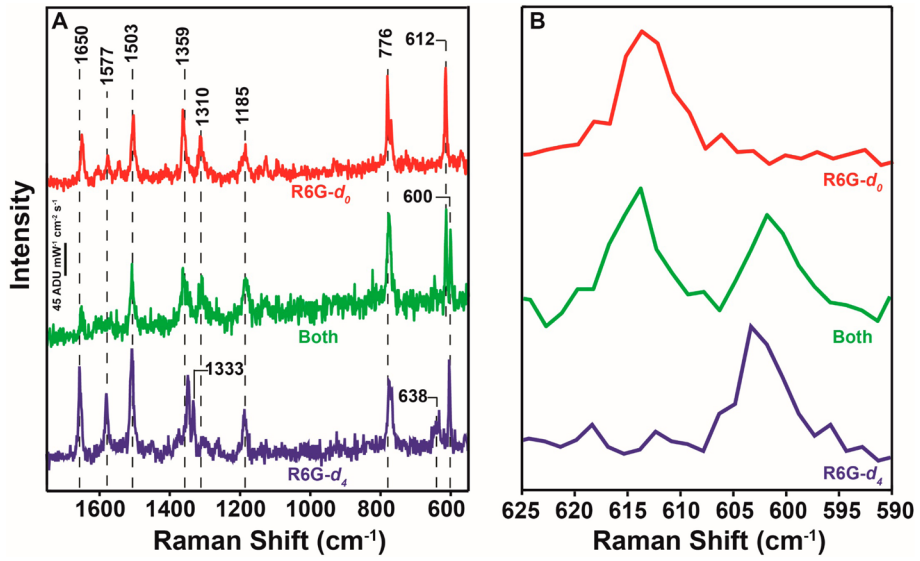

Figure 4. (A) Representative SMSERS spectra of R6G-d_0 (red), both (green), and R6G-d_4 (blue). (B) SMSERS spectra focused on the 600 cm^{-1} region, displaying the unique isotopologue spectral features for R6G-d_0 (red) and R6G-d_4 (blue). Data acquisition parameters for SMSERS measurements were the following: λ_{ex} = 532 nm, P_{ex} = 13.6 mW, t_{acq} = 3 s.

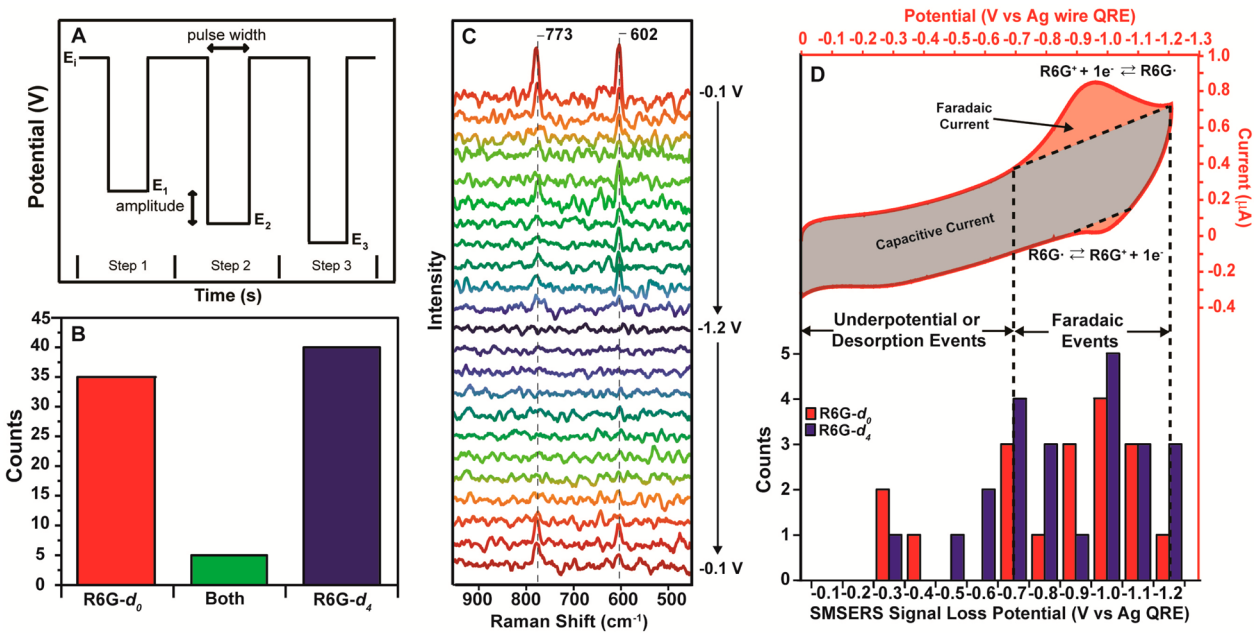

Figure 5. (A) Representative trace of the potential step function applied in electrochemistry measurements to each single Ag nanoparticle aggregate, where E_i = 0 V, E_1 = −0.1 V. The amplitude between steps is −0.1 V, and the pulse width is equivalent to the spectral acquisition time. (B) Histogram displaying all SMSERS events. (C) Representative SMSERS spectra from a single particle aggregate displaying signal change as a function of applied potential. The SMSERS signal is lost at −1.2 V (center, dark blue trace) and returns at −0.2 V (bottom, red trace). (D) Surface CV of high coverage R6G on a polished Ag disk electrode in 100 mM TBAP in MeCN (top) compared to the histogram of all SMSERS measured signal loss events (bottom).

electrochemical events occurring, and therefore there should be no SMSERS signal loss with the potential step. In this experiment, 16 of 20 SMSERS spectra collected showed no signal loss during the potential step; the consistent SMSERS signal indicates that neither R6G cation desorption (eq 2) nor electrochemical reduction followed by radical desorption (eq 3) occurred (Figure 6A). Of the 20 SMSERS spectra collected, 4 showed signal loss between −0.4 V and −0.7 V as illustrated in Figure 6B, which could be caused by eq 2 or eq 3. We are inclined to think that these four cases were most likely reduction events followed by diffusion of the radical as represented by eq 3. Due to the fact that at this control experiment we do not observe any signal loss at −0.3 V, we assume that the loss events observed at −0.3 V in Figure 5D are most likely caused by desorption of the R6G cation (eq 2) and we hypothesize that the complete SMSERS signal loss between −0.6 V and −1.2 V, without signal return or oxidation, is probably due to electrochemical desorption of the R6G neutral radical (eq 3).

We observe a broadened SMSERS signal loss potential distribution (Figure 5D) relative to the Faradaic region in the surface CV. In light of this, we now discuss the origin of the

DOI: 10.1021/acs.jpcc.5b10652
J. Phys. Chem. C 2015, 119, 28226−28234

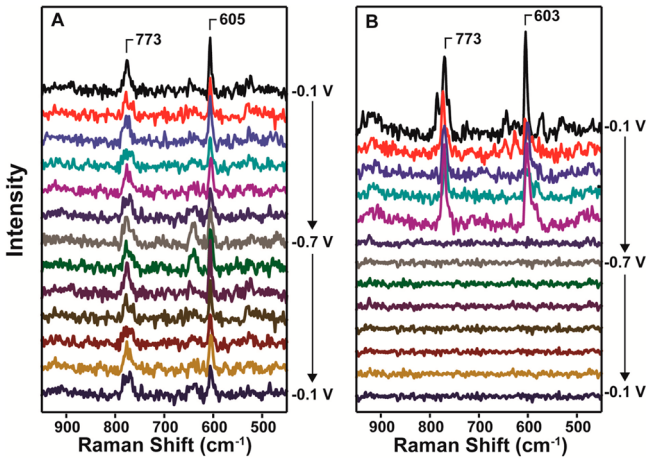

Figure 6. SMSERS spectra from potential steps in the non-Faradaic region (−0.1 to −0.7 V). (A) Spectra display no loss in SMSER signal, illustrative example of 16 out of 20 events, indicating that neither eq 2 nor eq 3 took place. (B) Representative SMSERS spectra for 4 out of 20 events where the potential step in the non-Faradaic region displays a loss in SMSER signal, here at −0.6 V. These SMSERS signal loss events are most likely due to electrochemical reduction of R6G and not R6G cation desorption.

broadened distribution of the SMSERS R6G signal loss potential histogram. For example, a similar broadening effect has been observed in a SMSERS experiment across a smaller potential range for an aqueous two electron, two proton transfer of Nile blue (NB) from Cortés et al.[1,44] The authors found a correlation between the peak positions of the 590 cm^{-1} ring breathing mode in NB to the reduction potential. They attribute this phenomenon to molecular orientation and the molecule's relative interaction strength with the nanoparticle surface. Additionally, another study by Salverda et al. found that when azurin, a Cu protein, is bound on Au electrodes at low coverage, the electron transfer rates were broadly distributed, which they attributed to heterogeneous protein orientation.[10] On the basis of these preceding studies and our experimental results, we propose two primary contributing factors to the observed broadened potential distribution: molecular reorientation on the surface and variations in the local hot-spot nanostructure or surface chemical potential, including in the former possible effects from varied curvatures and possible oxide layers.

We note that we do not attempt to extract information on the molecular position on the surface from the relative intensities of the SMSERS signal. Commonly, the intensity of SERS spectra will decay accordingly with the distance of the Raman molecule to the substrate.[52] Distinctly, at the single molecule level, the intensity of the peaks might change due to the distance or relative position of the molecule to the hot spot or variations in its excited-state properties.[53] To this end, we analyze the R6G peak positions as a function of potential, which is sensitive to position relative to the Ag NP surface.

To simplify the spectral analysis, we divide it into two regions. First, we examine the 600 cm^{-1} region R6G peak, which has been determined by DFT calculations to be a ring breathing mode.[54] While the position of the mode varies from spectrum to spectrum, we do not observe any correlation between the applied potential and peak position shift. Also, there is no connection between peak position and the potential of an SMSERS signal loss event when correlating the data in Figure 5D to that of Figure S6A. Then, we examined the 1350 cm^{-1} region mode, determined by DFT calculations to have 93.9% ethylamine moiety vibrational character and hypothesized as the anchoring moiety.[54] If R6G binds to the Ag nanoparticle surface via the ethylamine moiety, its corresponding vibrational mode peak position should therefore be sensitive to changes in the orientation relative to the Ag nanoparticle. In half of the spectra collected, there is a blue shift of the 1350 cm^{-1} mode with increasingly applied negative potential (Figure S5). Yet, there is no correlation between the peak position and the reduction or signal loss potential when correlating the data from Figure 5D to Figure S6B. The shifts observed in the 1350 cm^{-1} mode could be attributed to a vibrational Stark effect, which occurs when a molecular dipole is perturbed by a local electric field.[55−57] Hence, the major difference between our results and Cortés et al.[44] is lack of a distinct correlation between Raman shift of either the 600 or 1350 cm^{-1} modes and the applied or reduction potential. Disregarding the difference in the spectral resolution because our measurements were performed with a lower spectral resolution, our results suggest that molecular orientation and interaction with the nanoparticle surface are not the only contributors to the broad SMSERS signal loss potential histogram.

We hypothesize that the major contribution to the broadened SMSERS signal loss potential distribution relative to the bulk is due to the local radius of curvature, surface site, and corresponding surface chemical potential of the specific site of the Ag nanoparticle where the R6G molecule is bound. Preceding theoretical and experimental studies indicate the structure-dependent electrochemical behavior of Ag nanostructures and that sharp, small radius of curvature features are the most electrochemically active.[58−61] For example, Zhang et al. measured the electrochemical oxidation of Ag nanotriangles and found that as a positive potential is applied to the substrate, the sharp, bottom edges first oxidize, followed by the more rounded triangular tip regions.[62] This behavior was rationalized based on a previous statement that the work function of a small, metallic particle varies inversely with the radius of a metallic nanoparticle. Recent work has also demonstrated the heterogeneous chemical activity of various nanoparticle shapes and sizes on the single particle level and supports the idea that electrochemical activity is dependent on surface structure.[63,64] We can extend these ideas to our findings, postulating that particles with smaller radii of curvature, or sharper nanofeatures, will be more electrochemically active and therefore lead to SMSERS underpotential events. For our SMSERS measurements, the subtle difference in local surface site structure, binding geometry, and overall nanoparticle shape and size can be a possible explanation of the lack of correlation between the broad potential range of SMSERS signal loss events and the Raman shifts observed.

4. CONCLUSIONS

In summary, we first characterize the bulk electrochemistry of R6G, which undergoes single electron redox. Next, we characterize the spectroelectrochemical response of the R6G electron transfer reaction with absorbance spectroscopy and SERS at high R6G coverage. Finally, we demonstrate the first observation of single-electron transfer with EC-SMSERS. The potential distribution of SMSERS signal loss events is broader than of the bulk electrochemical system. We attribute this behavior to variations in molecular orientations and variations

DOI: 10.1021/acs.jpcc.5b10652
J. Phys. Chem. C 2015, 119, 28226−28234

in the radius of curvature, binding site, and/or chemical potential where the R6G molecule is bound to the Ag nanoparticle substrate. Future efforts will address the correlation of SMSERS measurements with electron microscopy to understand the impact of nanofeatures on the distribution of reduction potentials together with density functional theory calculations. Overall, this work has presented challenges involved in studying single-molecule single-electron electrochemical events through SERS and pursuing electrochemical control at the nanoscale.

■ ASSOCIATED CONTENT

Supporting Information

The Supporting Information is available free of charge on the ACS Publications website at DOI: 10.1021/acs.jpcc.5b10652.

Additional spectral and electrochemical characterization data, photographs of the custom glass cell, supplementary SMSERS spectra (PDF)

■ AUTHOR INFORMATION

Corresponding Author

*E-mail: vanduyne@northwestern.edu.

Author Contributions

All authors have given approval to the final version of the manuscript.

Notes

The authors declare no competing financial interest.

■ ACKNOWLEDGMENTS

This work was supported by Air Force Office of Scientific Research MURI (Grant FA9550-14-1-0003) and the National Science Foundation (MRSEC Grants NSF DMR-1121262 and NSF CHE-1152547). This work made use of the EPIC facility (NUANCE Center—Northwestern University), which has received support from the MRSEC program (Grant NSF DMR-1121262) at the Materials Research Center; the Nanoscale Science and Engineering Center (Grant NSF EEC-0647560) at the International Institute for Nanotechnology; and the State of Illinois, through the International Institute for Nanotechnology. M.F.C. acknowledges the access to the solvent system of the Stoddart group at Northwestern University for the provided dried acetonitrile.

■ REFERENCES

(1) Cortés, E.; Etchegoin, P. G.; Le Ru, E. C.; Fainstein, A.; Vela, M. E.; Salvarezza, R. C. Monitoring the Electrochemistry of Single Molecules by Surface-Enhanced Raman Spectroscopy. *J. Am. Chem. Soc.* **2010**, *132*, 18034−18037.

(2) Venkataraman, L.; Klare, J. E.; Nuckolls, C.; Hybertsen, M. S.; Steigerwald, M. L. Dependence of Single-Molecule Junction Conductance on Molecular Conformation. *Nature* **2006**, *442*, 904−907.

(3) Shan, X.; Patel, U.; Wang, S.; Iglesias, R.; Tao, N. Imaging Local Electrochemical Current Via Surface Plasmon Resonance. *Science* **2010**, *327*, 1363−1366.

(4) Wilson, A. J.; Willets, K. A. Visualizing Site-Specific Redox Potentials on the Surface of Plasmonic Nanoparticle Aggregates with Superlocalization SERS Microscopy. *Nano Lett.* **2014**, *14*, 939−45.

(5) Mao, X.; Hatton, T. A. Recent Advances in Electrocatalytic Reduction of Carbon Dioxide Using Metal-Free Catalysts. *Ind. Eng. Chem. Res.* **2015**, *54*, 4033−4042.

(6) Lipson, A. L.; Puntambekar, K.; Comstock, D. J.; Meng, X.; Geier, M. L.; Elam, J. W.; Hersam, M. C. Nanoscale Investigation of Solid Electrolyte Interphase Inhibition on Li-Ion Battery MnO Electrodes Via Atomic Layer Deposition of Al_2O_3. *Chem. Mater.* **2014**, *26*, 935−940.

(7) Lipson, A. L.; Ginder, R. S.; Hersam, M. C. Nanoscale *in situ* Characterization of Li-Ion Battery Electrochemistry Via Scanning Ion Conductance Microscopy. *Adv. Mater.* **2011**, *23*, 5613−7.

(8) Yu; Chang, S.-S.; Lee, C.-L.; Wang, C. R. C. Gold Nanorods: Electrochemical Synthesis and Optical Properties. *J. Phys. Chem. B* **1997**, *101*, 6661−6664.

(9) Taberna, P. L.; Mitra, S.; Poizot, P.; Simon, P.; Tarascon, J. M. High Rate Capabilities Fe_3O_4-Based Cu Nano-Architectured Electrodes for Lithium-Ion Battery Applications. *Nat. Mater.* **2006**, *5*, 567−573.

(10) Salverda, J. M.; Patil, A. V.; Mizzon, G.; Kuznetsova, S.; Zauner, G.; Akkilic, N.; Canters, G. W.; Davis, J. J.; Heering, H. A.; Aartsma, T. J. Fluorescent Cyclic Voltammetry of Immobilized Azurin: Direct Observation of Thermodynamic and Kinetic Heterogeneity. *Angew. Chem., Int. Ed.* **2010**, *49*, 5776−9.

(11) Davis, J. J.; Burgess, H.; Zauner, G.; Kuznetsova, S.; Salverda, J.; Aartsma, T.; Canters, G. W. Monitoring Interfacial Bioelectrochemistry Using a FRET Switch. *J. Phys. Chem. B* **2006**, *110*, 20649−20654.

(12) Goldsmith, R. H.; Tabares, L. C.; Kostrz, D.; Dennison, C.; Aartsma, T. J.; Canters, G. W.; Moerner, W. E. Redox Cycling and Kinetic Analysis of Single Molecules of Solution-Phase Nitrite Reductase. *Proc. Natl. Acad. Sci. U. S. A.* **2011**, *108*, 17269−74.

(13) Fan, F.-R. F.; Bard, A. J. Electrochemical Detection of Single Molecules. *Science* **1995**, *267*, 871−874.

(14) Huang, K.-C.; White, R. J. Random Walk on a Leash: A Simple Single-Molecule Diffusion Model for Surface-Tethered Redox Molecules with Flexible Linkers. *J. Am. Chem. Soc.* **2013**, *135*, 12808−12817.

(15) Zhang, J.; Kuznetsov, A. M.; Medvedev, I. G.; Chi, Q.; Albrecht, T.; Jensen, P. S.; Ulstrup, J. Single-Molecule Electron Transfer in Electrochemical Environments. *Chem. Rev.* **2008**, *108*, 2737−2791.

(16) Kang, S.; Nieuwenhuis, A. F.; Mathwig, K.; Mampallil, D.; Lemay, S. G. Electrochemical Single-Molecule Detection in Aqueous Solution Using Self-Aligned Nanogap Transducers. *ACS Nano* **2013**, *7*, 10931−10937.

(17) Lemay, S. G.; Kang, S.; Mathwig, K.; Singh, P. S. Single-Molecule Electrochemistry: Present Status and Outlook. *Acc. Chem. Res.* **2013**, *46*, 369−377.

(18) Hill, C. M.; Clayton, D. A.; Pan, S. Combined Optical and Electrochemical Methods for Studying Electrochemistry at the Single Molecule and Single Particle Level: Recent Progress and Perspectives. *Phys. Chem. Chem. Phys.* **2013**, *15*, 20797−20807.

(19) Lei, C.; Hu, D.; Ackerman, E. J. Single-Molecule Fluorescence Spectroelectrochemistry of Cresyl Violet. *Chem. Commun.* **2008**, 5490−2.

(20) Chang, Y.-L.; Palacios, R. E.; Fan, F.-R. F.; Bard, A. J.; Barbara, P. F. Electrogenerated Chemiluminescence of Single Conjugated Polymer Nanoparticles. *J. Am. Chem. Soc.* **2008**, *130*, 8906−8907.

(21) Tao, N. J. Probing Potential-Tuned Resonant Tunneling Through Redox Molecules with Scanning Tunneling Microscopy. *Phys. Rev. Lett.* **1996**, *76*, 4066−4069.

(22) Nie, S.; Emory, S. R. Probing Single Molecules and Single Nanoparticles by Surface-Enhanced Raman Scattering. *Science* **1997**, *275*, 1102−1106.

(23) Blackie, E.; Le Ru, E. C.; Meyer, M.; Timmer, M.; Burkett, B.; Northcote, P.; Etchegoin, P. G. Bi-Analyte SERS with Isotopically Edited Dyes. *Phys. Chem. Chem. Phys.* **2008**, *10*, 4147−4153.

(24) Etchegoin, P. G.; Le Ru, E. C.; Fainstein, A. Bi-Analyte Single Molecule SERS Technique with Simultaneous Spatial Resolution. *Phys. Chem. Chem. Phys.* **2011**, *13*, 4500−4506.

(25) Dieringer, J. A.; Lettan, R. B.; Scheidt, K. A.; Van Duyne, R. P. A Frequency Domain Existence Proof of Single-Molecule Surface-Enhanced Raman Spectroscopy. *J. Am. Chem. Soc.* **2007**, *129*, 16249−16256.

(26) Kleinman, S. L.; Ringe, E.; Valley, N.; Wustholz, K. L.; Phillips, E.; Scheidt, K. A.; Schatz, G. C.; Van Duyne, R. P. Single-Molecule

DOI: 10.1021/acs.jpcc.5b10652
J. Phys. Chem. C 2015, 119, 28226−28234

Surface-Enhanced Raman Spectroscopy of Crystal Violet Isotopologues: Theory and Experiment. *J. Am. Chem. Soc.* **2011**, *133*, 4115−4122.
(27) Blackie, E. J.; Ru, E. C. L.; Etchegoin, P. G. Single-Molecule Surface-Enhanced Raman Spectroscopy of Nonresonant Molecules. *J. Am. Chem. Soc.* **2009**, *131*, 14466−14472.
(28) Etchegoin, P. G.; Le Ru, E. C.; Meyer, M. Evidence of Natural Isotopic Distribution from Single-Molecule SERS. *J. Am. Chem. Soc.* **2009**, *131*, 2713−2716.
(29) Stranahan, S. M.; Willets, K. A. Super-Resolution Optical Imaging of Single-Molecule SERS Hot Spots. *Nano Lett.* **2010**, *10*, 3777−84.
(30) Artur, C.; Le Ru, E. C.; Etchegoin, P. G. Temperature Dependence of the Homogeneous Broadening of Resonant Raman Peaks Measured by Single-Molecule Surface-Enhanced Raman Spectroscopy. *J. Phys. Chem. Lett.* **2011**, *2*, 3002−3005.
(31) Le Ru, E. C.; Etchegoin, P. G. Single-Molecule Surface-Enhanced Raman Spectroscopy. *Annu. Rev. Phys. Chem.* **2012**, *63*, 65−87.
(32) Patra, P. P.; Chikkaraddy, R.; Tripathi, R. P.; Dasgupta, A.; Kumar, G. V. Plasmofluidic Single-Molecule Surface-Enhanced Raman Scattering from Dynamic Assembly of Plasmonic Nanoparticles. *Nat. Commun.* **2014**, *5*, 4357.
(33) Ahmed, A.; Gordon, R. Single Molecule Directivity Enhanced Raman Scattering Using Nanoantennas. *Nano Lett.* **2012**, *12*, 2625−2630.
(34) Crozier, K. B.; Wenqi, Z.; Dongxing, W.; Shiyun, L.; Best, M. D.; Camden, J. P. Plasmonics for Surface Enhanced Raman Scattering: Nanoantennas for Single Molecules. *IEEE J. Sel. Top. Quantum Electron.* **2014**, *20*, 152−162.
(35) Zrimsek, A. B.; Henry, A.-I.; Van Duyne, R. P. Single Molecule Surface-Enhanced Raman Spectroscopy Without Nanogaps. *J. Phys. Chem. Lett.* **2013**, *4*, 3206−3210.
(36) Sonntag, M. D.; Klingsporn, J. M.; Garibay, L. K.; Roberts, J. M.; Dieringer, J. A.; Seideman, T.; Scheidt, K. A.; Jensen, L.; Schatz, G. C.; Van Duyne, R. P. Single-Molecule Tip-Enhanced Raman Spectroscopy. *J. Phys. Chem. C* **2012**, *116*, 478−483.
(37) Steidtner, J.; Pettinger, B. Tip-Enhanced Raman Spectroscopy and Microscopy on Single Dye Molecules with 15 nm Resolution. *Phys. Rev. Lett.* **2008**, *100*, 236101.
(38) Etchegoin, P. G.; Meyer, M.; Le Ru, E. C. Statistics of Single Molecule SERS Signals: Is There a Poisson Distribution of Intensities? *Phys. Chem. Chem. Phys.* **2007**, *9*, 3006−3010.
(39) Dieringer, J. A.; Wustholz, K. L.; Masiello, D. J.; Camden, J. P.; Kleinman, S. L.; Schatz, G. C.; Van Duyne, R. P. Surface-Enhanced Raman Excitation Spectroscopy of a Single Rhodamine 6G Molecule. *J. Am. Chem. Soc.* **2009**, *131*, 849−854.
(40) Titus, E. J.; Weber, M. L.; Stranahan, S. M.; Willets, K. A. Super-Resolution SERS Imaging Beyond the Single-Molecule Limit: An Isotope-Edited Approach. *Nano Lett.* **2012**, *12*, 5103−5110.
(41) Mirsaleh-Kohan, N.; Iberi, V.; Simmons, P. D.; Bigelow, N. W.; Vaschillo, A.; Rowland, M. M.; Best, M. D.; Pennycook, S. J.; Masiello, D. J.; Guiton, B. S.; et al. Single-Molecule Surface-Enhanced Raman Scattering: Can STEM/EELS Image Electromagnetic Hot Spots? *J. Phys. Chem. Lett.* **2012**, *3*, 2303−2309.
(42) Galloway, C. M.; Le Ru, E. C.; Etchegoin, P. G. Single-Molecule Vibrational Pumping in SERS. *Phys. Chem. Chem. Phys.* **2009**, *11*, 7372−7380.
(43) Fu, Y.; Dlott, D. D. Single Molecules under High Pressure. *J. Phys. Chem. C* **2015**, *119*, 6373−6381.
(44) Cortes, E.; Etchegoin, P. G.; Le Ru, E. C.; Fainstein, A.; Vela, M. E.; Salvarezza, R. C. Strong Correlation between Molecular Configurations and Charge-Transfer Processes Probed at the Single-Molecule Level by Surface-Enhanced Raman Scattering. *J. Am. Chem. Soc.* **2013**, *135*, 2809−15.
(45) Wang, Y.; Sevinc, P. C.; He, Y.; Lu, H. P. Probing Ground-State Single-Electron Self-Exchange across a Molecule−Metal Interface. *J. Am. Chem. Soc.* **2011**, *133*, 6989−6996.
(46) Zhang, D.; Xie, Y.; Deb, S. K.; Davison, V. J.; Ben-Amotz, D. Isotope Edited Internal Standard Method for Quantitative Surface-Enhanced Raman Spectroscopy. *Anal. Chem.* **2005**, *77*, 3563−3569.
(47) Lee, P. C.; Meisel, D. Adsorption and Surface-Enhanced Raman of Dyes on Silver and Gold Sols. *J. Phys. Chem.* **1982**, *86*, 3391−3395.
(48) Bard, A. J.; Faulkner, L. R. *Electrochemical Methods: Fundamentals and Applications*, 2nd ed.; Wiley, 2000; p 864.
(49) Jäckel, F.; Kinkhabwala, A. A.; Moerner, W. E. Gold Bowtie Nanoantennas for Surface-Enhanced Raman Scattering under Controlled Electrochemical Potential. *Chem. Phys. Lett.* **2007**, *446*, 339−343.
(50) Shegai, T.; Vaskevich, A.; Rubinstein, I.; Haran, G. Raman Spectroelectrochemistry of Molecules within Individual Electromagnetic Hot Spots. *J. Am. Chem. Soc.* **2009**, *131*, 14390−8.
(51) Redmond, P. L.; Hallock, A. J.; Brus, L. E. Electrochemical Ostwald Ripening of Colloidal Ag Particles on Conductive Substrates. *Nano Lett.* **2005**, *5*, 131−5.
(52) Dieringer, J. A.; McFarland, A. D.; Shah, N. C.; Stuart, D. A.; Whitney, A. V.; Yonzon, C. R.; Young, M. A.; Zhang, X.; Van Duyne, R. P. Surface Enhanced Raman Spectroscopy: New Materials, Concepts, Characterization Tools, and Applications. *Faraday Discuss.* **2006**, *132*, 9−26.
(53) Sonntag, M. D.; Chulhai, D.; Seideman, T.; Jensen, L.; Van Duyne, R. P. The Origin of Relative Intensity Fluctuations in Single-Molecule Tip-Enhanced Raman Spectroscopy. *J. Am. Chem. Soc.* **2013**, *135*, 17187−17192.
(54) Klingsporn, J. M.; Jiang, N.; Pozzi, E. A.; Sonntag, M. D.; Chulhai, D.; Seideman, T.; Jensen, L.; Hersam, M. C.; Van Duyne, R. P. Intramolecular Insight into Adsorbate-Substrate Interactions Via Low-Temperature, Ultrahigh-Vacuum Tip-Enhanced Raman Spectroscopy. *J. Am. Chem. Soc.* **2014**, *136*, 3881−7.
(55) Bublitz, G. U.; Boxer, S. G. Stark Spectroscopy: Applications in Chemistry, Biology, and Materials Science. *Annu. Rev. Phys. Chem.* **1997**, *48*, 213−242.
(56) Andrews, S. S.; Boxer, S. G. Vibrational Stark Effects of Nitriles I. Methods and Experimental Results. *J. Phys. Chem. A* **2000**, *104*, 11853−11863.
(57) Andrews, S. S.; Boxer, S. G. Vibrational Stark Effects of Nitriles II. Physical Origins of Stark Effects from Experiment and Perturbation Models. *J. Phys. Chem. A* **2002**, *106*, 469−477.
(58) Makov, G.; Nitzan, A.; Brus, L. E. On the Ionization Potential of Small Metal and Dielectric Particles. *J. Chem. Phys.* **1988**, *88*, 5076.
(59) Plieth, W. J. Electrochemical Properties of Small Clusters of Metal Atoms and Their Role in the Surface Enhanced Raman Scattering. *J. Phys. Chem.* **1982**, *86*, 3166−3170.
(60) Ivanova, O. S.; Zamborini, F. P. Electrochemical Size Discrimination of Gold Nanoparticles Attached to Glass/Indium−Tin-Oxide Electrodes by Oxidation in Bromide-Containing Electrolyte. *Anal. Chem.* **2010**, *82*, 5844−5850.
(61) Ivanova, O. S.; Zamborini, F. P. Size-Dependent Electrochemical Oxidation of Silver Nanoparticles. *J. Am. Chem. Soc.* **2010**, *132*, 70−72.
(62) Zhang, X.; Hicks, E. M.; Zhao, J.; Schatz, G. C.; Van Duyne, R. P. Electrochemical Tuning of Silver Nanoparticles Fabricated by Nanosphere Lithography. *Nano Lett.* **2005**, *5*, 1503−1507.
(63) Shen, H.; Zhou, X.; Zou, N.; Chen, P. Single-Molecule Kinetics Reveals a Hidden Surface Reaction Intermediate in Single-Nanoparticle Catalysis. *J. Phys. Chem. C* **2014**, *118*, 26902−26911.
(64) Patil, A. V.; Davis, J. J. Visualizing and Tuning Thermodynamic Dispersion in Metalloprotein Monolayers. *J. Am. Chem. Soc.* **2010**, *132*, 16938−16944.

DOI: 10.1021/acs.jpcc.5b10652
J. Phys. Chem. C 2015, 119, 28226−28234